SCIEPublish

Article

Eastern Lubber Grasshopper Extract-Inspired Silver Nanoparticles Selectively Inhibit Methicillin-Resistant *Staphylococcus aureus*

Lauren Hanna Sloneker [1], William Joseph Dodson [2], Yacoub Qamar [1], William Yang [1], Hunter Michael Salvatore Galmiche [2] and James Lee Cho [2,*]

[1] Department of Biological Sciences, Southeastern Louisiana University, Hammond, LA 70402, USA; lauren.hanna@selu.edu (L.H.S.); yacoub.qamar@selu.edu (Y.Q.); william.yang@selu.edu (W.Y.)

[2] Department of Chemistry and Physics, Southeastern Louisiana University, Hammond, LA 70402, USA; william.dodson@selu.edu (W.J.D.); hunter.galmiche@selu.edu (H.M.S.G.)

* Corresponding author. E-mail: james.cho@selu.edu (J.L.C.)

Received: 4 June 2025; Accepted: 30 July 2025; Available online: 1 August 2025

ABSTRACT: Silver nanoparticles (AgNPs) were synthesized using a protein/polypeptide-rich aqueous extract from the Eastern lubber grasshopper (*Romalea microptera*), as a natural reducing and capping agent. The resulting AgNPs exhibited relatively uniform sizes (10–60 nm) and were characterized by Fourier Transform Infrared Spectroscopy (FTIR), Ultraviolet-visible (UV-Vis) spectroscopy, Transmission electron microscopy (TEM), and Scanning Electron Microscopy (SEM). Disk diffusion tests against five bacterial strains (Methicillin-resistant *Staphylococcus aureus* (MRSA), *Burkholderia cenocepacia*, *Klebsiella pneumoniae*, *Pseudomonas aeruginosa*, and *Escherichia coli*) demonstrated that the insect-extract-induced AgNPs selectively and significantly inhibited MRSA growth, with an average value of zone of inhibition of 9.16 ± 1.11 mm (n = 4). Statistical analysis confirmed the superior antibacterial activity of the Eastern lubber grasshopper-derived AgNPs against MRSA compared to citrate-capped AgNPs and free silver ions. These findings reveal the potential of insect-derived AgNPs as selective, green-synthesized antibacterial agents with enhanced efficacy and reduced side effects, particularly against antibiotic-resistant pathogens.

Keywords: Silver nanoparticle assembly; Eastern lubber grasshopper; Bio-inspired synthesis; Nano-biomaterials; Selective antibacterial activity

© 2025 The authors. This is an open access article under the Creative Commons Attribution 4.0 International License (https://creativecommons.org/licenses/by/4.0/).

1. Introduction

Recently, *Staphylococcus aureus* has posed a significant public health threat due to its enhanced antibiotic resistance [1]. It is associated with severe infections in individuals. According to the Centers for Disease Control and Prevention (CDC), *Staphylococcus aureus* is a bacterium that causes skin and soft tissue infections. More than 119,000 bloodstream staph infections occurred in 2017, and nearly 20,000 people died from bloodstream staph infections in 2017 in the United States [2]. Its ability to spread rapidly in community and healthcare settings underscores the urgent need for effective treatments [3]. The persistence and adaptability of this strain emphasize the critical necessity for novel therapeutic strategies to combat Staphylococcus aureus and mitigate its impact on public health.

Silver nanoparticles (AgNPs) are widely recognized for their potent antibacterial effects against numerous pathogenic bacteria [4]. AgNPs induce reactive oxygen species (ROS) production, causing oxidative stress. This oxidative stress is mainly triggered by the release of silver (I) ions (Ag^+), resulting from the re-oxidation of metallic AgNPs [5]. The potency of this antibacterial activity largely depends on the nature of the capping agents coating the surface of the AgNPs [6]. Biological compounds, including polypeptides and proteins, can be excellent capping agents, enhancing additional or selective antibacterial activities [7].

Insect extracts are rich in a variety of biomolecules, including proteins, peptides, and amino acids, which possess reducing properties [8]. These biomolecules facilitate the reduction of metal ions by acting as reducing agents by donating electrons to transform metal ions into metal nanoparticles [9]. The Eastern lubber grasshopper (ELG) (*Romalea microptera*) is one of the most common grasshoppers in the southeastern area of the United States of America

and elsewhere in the world [10]. The Eastern lubber grasshopper's high protein content and overall body composition produce an aqueous extract rich in water-soluble compounds and biological polymers. This includes hydrophilic polypeptides, proteins, and potentially other bioactive compounds such as DNA, polyphenols, flavonoids, and terpenoids, depending on the specific biochemical makeup of the ELG. Although the Eastern lubber grasshopper (*Romalea microptera*) has not been extensively studied for direct antimicrobial properties, previous studies have reported that many edible insects possess inherent bioactivity due to their protein, peptide, and phenolic content [11,12]. Given its herbivorous diet and high protein content, ELG may accumulate or produce bioactive compounds capable of reducing metal ions and enhancing selective antimicrobial activity, making it a compelling choice for bioinspired nanomaterial synthesis.

In this article, we report the synthesis of AgNPs using aqueous eastern lubber grasshopper extract (AELGE). The disk diffusion test showed that AELGE-induced AgNPs (AELGE-AgNPs) selectively inhibited the growth of *Staphylococcus aureus* USA300, a particularly virulent strain of Methicillin-resistant *Staphylococcus aureus* (MRSA), among five bacteria (*Burkholderia cenocepacia* K-56 (BC), *Klebsiella pneumoniae* ST258 (KP), *Pseudomonas aeruginosa* PAO1 (PA), and *Staphylococcus aureus* USA300 (MRSA or SA) and *Escherichia coli* HB101 K-12 (EC)). These results suggest that AELGE-AgNPs could be potential candidates for developing selective antibacterial agents through green chemical methods. Additionally, we proposed the rationale of the selective antibacterial activity (SAA) of the AELGE-AgNPs by suggesting possible interactions between the SA bacterial cell membrane and the protein/peptide-based capping agents present on the AELGE-AgNPs.

2. Materials and Methods

2.1. AELGE Preparation at Different Concentrations

A single Eastern lubber grasshopper (ELG) specimen was collected in Amite, LA, USA. The ELG, weighing 7.40 g, was combined with 150 mL of distilled water and blended (Figure S1). The resulting mixture was centrifuged at 4000 rpm for 50 min. The purified AELGE was then frozen at –70 °C and subsequently freeze-dried into a powder at −40 °C over 50–60 h using a Scientific Pro Freeze Dryer from HARVESTRIGHT. This AELGE powder was later re-dissolved in distilled water to obtain the desired concentration, which was confirmed via UV-Vis spectrophotometry (% *m*/*v* or mg/mL). (Freeze-drying was performed using low-temperature (−40 °C) vacuum sublimation to minimize potential denaturation).

2.2. FTIR/BCA/SDS Analysis

An FTIR spectrometer (Thermo Scientific, Waltham, MA, USA, Nicolet iS10, Smart iTX) was used to analyze the chemical components of AELGE solution and AELGE-AgNP solution. Spectra were collected in the wavenumber range of 800–4000 cm^{-1} with 16 scans. The presence and concentration of proteins in AELGE were confirmed and determined using the Pierce™ BCA Protein Assay Kit. For SDS-PAGE, AELGE (2.0%, 100 µL) was mixed with 100 µL of SDS-PAGE buffer and 7.0 µL of 2-Mercaptoethanol (BME, 14.7 M). The mixture was then heated at 90 °C for 10 min. Proteins in AELGE were separated in Mini-PROTEAN® TGXTM gel (4–20%) casted with a Mini-protean Tetra Vertical Electrophoresis Cell (Bio-Rad, Hercules, CA, USA) at 150 V for 35 min. Prestained Protein Standard (Bio-Rad) was used to monitor the sizes of proteins. The separated proteins in the SDS-polyacrylamide gel were stained with Bio-safe Coomassie Brilliant Blue G-250 dye for 24 h, with gentle shaking, with an orbital shaker, and treated with distilled water (destaining solution) with additional 24-h gentle shaking to locate the protein bands visually. (The retained bioactivity of AELGE after rehydration following the freeze-drying process was confirmed by successful nanoparticle formation, consistent FTIR spectra, and protein detection via BCA and SDS-PAGE, suggesting that the functional biomolecules remained largely intact).

2.3. Characterization of Synthesized AELGE-AgNPs

AgNPs were synthesized by mixing 300 µL of AELGE (1.0%) with 50 µL of Ag^+ ion solution ($AgNO_3$, 50 mM). The remaining AELGE protein concentration was measured after formation of the AgNPs. The AgNPs formed within 48 h at approximately 20 °C. The resulting aqueous AELGE-induced AgNP (AELGE-AgNP) solution was mixed with 1 mL of distilled water and vortexed and sonicated (for homogenization) for 1 min and stored at room temperature (20.0 °C) for later use. The presence of AgNPs was initially confirmed using a UV-Vis spectrometer (Thermo Evolution 220) and a Thermo Scientific™ NanoDrop™ OneC Microvolume UV-Vis Spectrophotometer. The UV-Vis spectra revealed a surface plasmon resonance (SPR) peak at approximately 440 nm, consistent with silver nanoparticle

formation. Based on the model proposed by Paramelle et al. (2014) [13], this SPR peak corresponds to an approximate nanoparticle size of 50 nm. This estimation complements our TEM-based size observations. Transmission electron microscopy (TEM) using a JEOL 2010 instrument operating at 200 kV, along with scanning electron microscopy (SEM) coupled with Energy-Dispersive X-ray Spectroscopy (EDX) on an FEI Quanta 650 FEG, was employed to characterize the AgNPs. To detect proteins in the capping agents of the AgNPs, 300 µL of AELGE was mixed with 50 µL of $AgNO_3$ solutions at different concentrations (20 mM, 50 mM, and 100 mM). These mixtures were labeled AELGE-20, AELGE-50, and AELGE-100, corresponding to the respective $AgNO_3$ concentrations. The mixtures were incubated at room temperature (20 °C) for approximately 30 h. Following incubation, the formed AgNPs were isolated by centrifugation at 14,000 rpm for 30 min using a Labnet Spectrafuge 16M Benchtop Micro-Centrifuge (Edison, NJ, USA). Subsequently, BCA assays were conducted to quantify the protein concentration remaining in the AELGE samples after AgNP isolation. (Note: All nanoparticle synthesis steps were performed at room temperature (~20°C) under normal ambient light. No additional UV or visible light source was used during the synthesis).

2.4. Synthesis of Citrate Induced AgNPs (Citrate-AgNPs) as a Control Group

Citrate-induced silver nanoparticles (Citrate-AgNPs) were synthesized using a modified Turkevich method. Fifty milliliters of aqueous silver nitrate ($AgNO_3$) solution (1.81 mM) was heated to 90 °C, just below boiling, with continuous stirring. Once the temperature reached approximately 90 °C, 100 µL of sodium citrate solution (10.0 M) was rapidly added to the $AgNO_3$ solution. The mixture was gently heated for 5–10 min, during which the color changed from clear to pale yellow and eventually to deep yellow-gray, indicating the formation of citrate-induced silver nanoparticles. After cooling to room temperature, the resulting citrate-AgNP colloid was stored in a glass bottle at 4 °C for further use.

2.5. Disk Diffusion Test of the AELGE-AgNPs

Each bacterial strain (*Burkholderia cenocepacia* K-56, *Escherichia coli* HB101 K-12, *Klebsiella pneumoniae* ST258, *Pseudomonas aeruginosa* PAO1, and *Staphylococcus aureus* USA300) was inoculated into 5.0 mL of Luria Broth (LB) medium and incubated overnight at 37 °C. Subsequently, a sterile spreader spread 50 µL of the overnight LB culture evenly onto Mueller-Hinton agar plates. Whatman AA discs (6 mm in diameter) were placed on the inoculated agar surfaces. A volume of 12 µL of the AELGE-AgNP solution was applied to each disc, and the plates were incubated for 24 h at 37 °C in a Thermo Scientific™ Heracell™ 150i incubator. Zones of inhibition (ZOIs) were measured in millimeters (mm) in diameter, excluding the 6 mm diameter of the disc. Areas of the zones of inhibition (AZOIs) were also calculated based on the ZOI measurements. For comparison, citrate-AgNPs were tested using the same disk diffusion method. Additionally, citrate-AgNPs + AELGE group was also tested (mixing 100 µL of AELGE (0.37%) with 900 µL of citrate-AgNP solution at 2.0 mM of Ag^+ ion) using the same disk diffusion method. Free Ag^+ ions (12 µL) at varying concentrations (0.50 mM, 4 mM, 7 mM, 10 mM, 15 mM, and 50 mM) were also tested to evaluate the antibacterial activity of silver alone in quantities comparable to those in the AELGE-AgNP samples. For statistical analysis, one-way analysis of variance (ANOVA) and Tukey HSD post-hoc test were used to validate the selective antibacterial activity (SAA) of AELGE-AgNPs against *Staphylococcus aureus* USA300 among the other tested bacteria (*B. cenocepacia, E. coli, K. pneumoniae,* and *P. aeruginosa*). An unpaired t-test was performed to assess the superiority of AELGE-AgNPs over citrate-AgNPs in terms of the overall antibacterial efficacy. (Zones of inhibition (ZOIs) were measured in millimeters (mm) using ImageJ software, excluding the 6 mm diameter of the disc. Each condition was tested in quadruplicate ($n = 4$)).

3. Results and Discussion

3.1. AELGE Component

The aqueous AELGE solution contains a mixture of water-soluble compounds extracted from the Eastern lubber grasshopper. In the infrared spectrum (Figure 1), two prominent peaks were observed near 3300 cm^{-1} and 1640 cm^{-1}, corresponding to the NH/OH stretching vibrations (including contributions from water molecules and the Amide A band) and the C=O bending vibrations (associated with water and the Amide I band), respectively [14,15]. The prominent OH band indicates the possible presence of other organic compounds with hydroxyl groups, such as polyphenols and flavonoids. Furthermore, the IR spectrum shows similarities to certain plant extracts. This could be explained by ELGs accumulating these compounds in their bodies through their herbivorous diet, primarily of plants.

Additionally, a noticeable shift in the FTIR spectrum was observed in the 500–600 cm^{-1} region between AELGE and AELGE-AgNPs. This shift, particularly near 520 cm^{-1}, may correspond to Ag-O or Ag-N bonding, providing further evidence for nanoparticle formation and interaction with the extract's functional groups [16].

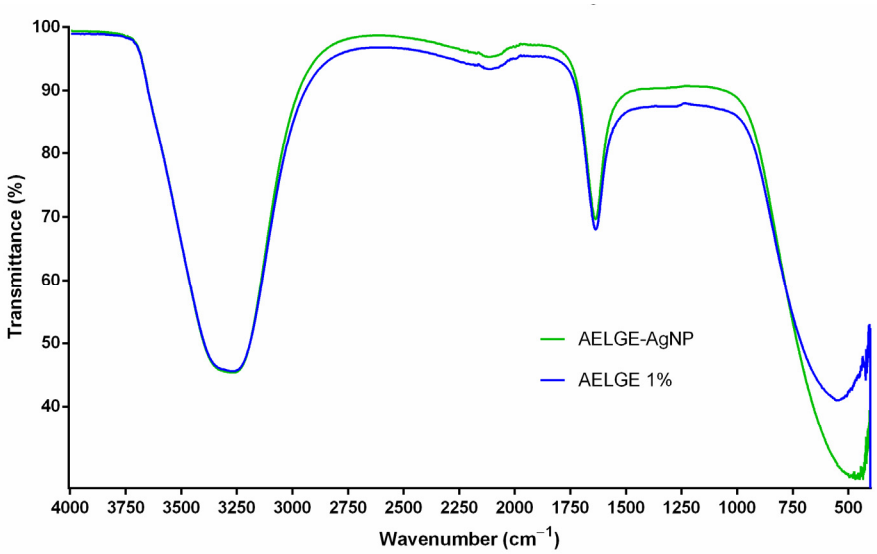

Figure 1. FTIR of AELGE and AELGE-AgNPs: Two main peaks indicate that AELGE and AELGE-AgNPs contain compounds with NH/OH groups (OH stretching of water plus Amide A band) and C=O groups (water bending plus Amide I band). These peaks suggest that AELGE and the capping agents of AELGE-AgNPs primarily comprise similar polypeptides and other water-soluble biomolecules, including phenols, alkaloids, and organic acids. Notably, the only substantial difference between the FTIR spectra of AELGE and AELGE-AgNPs was detected in the region below 750 cm^{-1}. This indicates that AELGE proteins and polypeptides underwent conformational changes in their structure while reducing Ag^+ ions to form AELGE-AgNPs.

AELGE-AgNPs also displayed an IR spectrum similar to that of AELGE, suggesting that protein/peptide-like compounds are the primary components. The IR spectrum of AELGE primarily shows characteristic absorptions linked to proteins and polypeptides. Furthermore, the only notable difference in the FTIR spectra of AELGE and AELGE-AgNPs appeared below 750 cm^{-1}, suggesting that the AELGE proteins and polypeptides experienced conformational changes during their reduction of Ag^+ ions to form AELGE-AgNPs. The Bicinchoninic Acid (BCA) assays also confirmed these IR findings. Protein-based biomolecules, including amino acids, peptides, and proteins, account for at least 42.0% of the total biological components in AELGE by mass (*m*/*v*). These protein-based constituents appear primarily as glycoproteins, as evidenced by the absence of distinct protein bands in the SDS-PAGE gel (Figure S2). The presence of glycoproteins may play a significant role in mediating nanoparticle-bacteria interactions, potentially enhancing selective binding to bacterial surfaces via sugar-protein or lectin-type interactions. This glycosylation may also influence AgNP dispersion stability and bioactivity, contributing to the observed selectivity against MRSA [17].

3.2. AELGE-Induced AgNP Characterization

Biological components in AELGE reacted with Ag^+ ions. They showed a yellow color to their metallic form due to surface plasmon resonance (SPR) within a day, and the AELGE-AgNP solution turns brown from initial yellow over days, as shown in Figure 2. The UV-Vis spectrum of the formed AgNPs further confirms their presence. Citrate-AgNPs were used as a control (Figure S3). Figure S3 shows the UV-Vis spectra of AELGE-AgNPs and Citrate-AgNPs. The broad absorption peak for AELGE-AgNPs appears around 440 nm within the 400–600 nm range, indicating that the average particle size is approximately 40–50 nm. In comparison, the broad peak for Citrate-AgNPs is centered around 455 nm, corresponding to an average particle size of approximately 60 nm [13]. However, it should be noted that size estimations based on UV-Vis spectra can be influenced by factors such as nanoparticle aggregation, shape, and surface chemistry, which may cause peak shifts or broadening [18]. Therefore, the presence of the formed AgNPs was also confirmed by TEM and SEM imaging methods (Figures 3 and S4). The AELGE-AgNPs, shown in Figure 3C, are relatively uniform in size, predominantly ranging from 3 to 11 nm, whereas the Citrate-AgNPs in Figure 3D exhibit a wider size distribution, spanning from 6 to 42 nm (Figure S5). The net surface charge of certain proteins (and/or polypeptides) and other biomolecules in AELGE is generally negative, primarily due to negatively charged functional groups. In addition, other electron-rich bio-organic compounds present in the AELGE solution likely contribute to the

reduction of Ag^+ ions into their nanoscale metallic form. The capping agents of AELGE-AgNPs include proteins derived from AELGE, as shown in Figures 4 and S6.

The synthesis mechanism involves the reduction of silver ions (Ag^+) by electron-donating biomolecules such as amino acids and polypeptides present in AELGE, followed by stabilization through capping by functional groups, including carboxyl, hydroxyl, amine, or thiol residues [7,19]. Although Ag^0 is the expected primary phase, prolonged synthesis time could lead to partial Ag_2O formation. Additionally, although TEM and SEM provided visual confirmation of morphology and size distribution, further long-term characterization using dynamic light scattering (DLS) and zeta potential measurements could provide insight into hydrodynamic size, surface charge, and colloidal stability of AELGE-AgNPs. These data are planned for inclusion in future studies to support Figure 3 and Figure S4 comparisons, and future studies will also include XRD analysis to confirm crystalline phases and estimate crystallite size via Scherrer's equation.

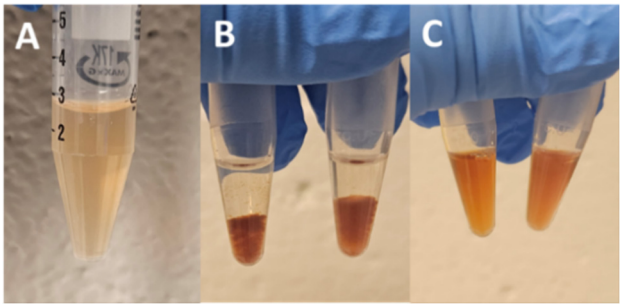

Figure 2. AgNP formation from AELGE-Ag^+ ion complex: (**A**) Silver (I) (Ag^+) ions were successfully reduced to their metallic form in the aqueous AELGE solution. The AELGE-AgNP solution initially exhibits a yellowish color within the first 24 h. (**B**) Over time, it gradually becomes more brownish, and large aggregated AgNP complexes settle at the bottom. (**C**) Vortexing and sonication can temporarily help maintain the AgNP solution in a colloidal state for a few minutes to hours, depending on the quantity of the formed AELGE-AgNPs.

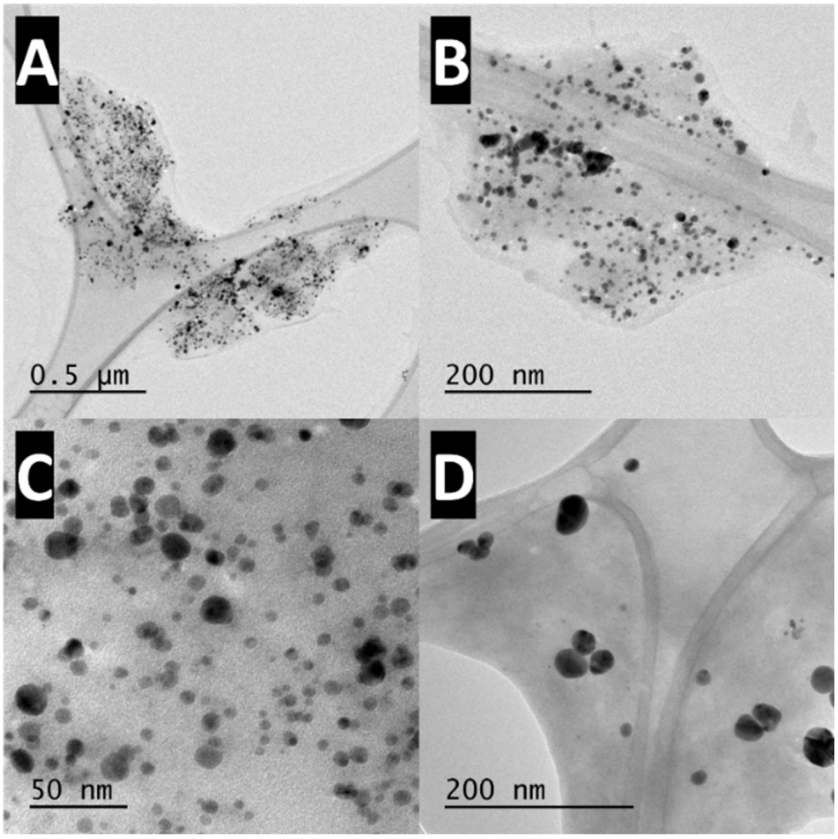

Figure 3. TEM images of AELGE-AgNPs: (**A**) AELGE-AgNPs are aggregated near biological bundles. (**B**) This image shows AELGE-AgNPs in biological aggregates at a higher magnification than in (**A**). (**C**) The sizes of the observed AELGE-AgNPs are fairly uniform, with most ranging from 5–25 nm in size. (**D**) TEM image of citrate-AgNPs.

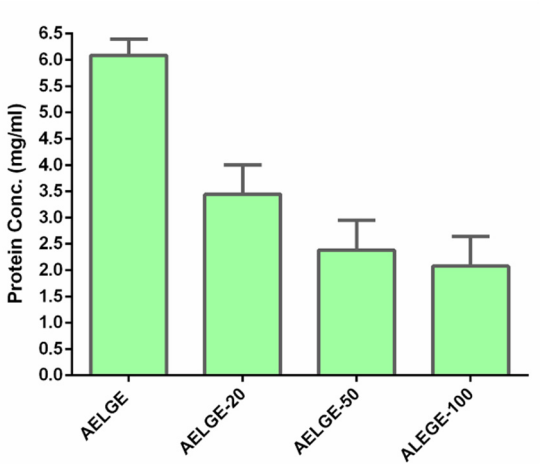

Figure 4. Protein concentration decreases after AELGE-AgNP separation: Proteins in AELGE decreased after the formed AELGE-AgNPs were separated by centrifugation. The measured protein concentrations in AELGE further declined as larger quantities of AgNPs were isolated, suggesting that the capping agents of the AgNPs include proteins derived from AELGE.

3.3. The Zones of Inhibition (ZOIs) of AELGE-AgNPs against Five Bacteria

The zones of inhibition (ZOIs) of the AELGE-AgNPs on the discs against five bacterial strains were measured in millimeters. AELGE-AgNPs demonstrated inhibition against all five bacteria. The largest ZOI was observed against Methicillin-resistant *Staphylococcus aureus* USA300 (MRSA) (Figure 5). The synergetic ZOI was also measured and compared to the ZOI produced by an equivalent amount of free Ag^+ ion solution against the same bacteria (AELGE-AgNP ZOI minus free Ag^+ ion ZOI). The ZOI area (ZOIA) was also calculated in mm^2 to assess how effectively AELGE-AgNPs inhibited bacterial growth. Finally, the synergistic effect of AELGE components and silver in the AELGE-AgNP form, compared to Ag^+ ions, was estimated through further calculations. AELGE-AgNPs exhibited greater antibacterial activity than free Ag^+ ions, except against *Pseudomonas aeruginosa* (PA), as shown in Figure S7.

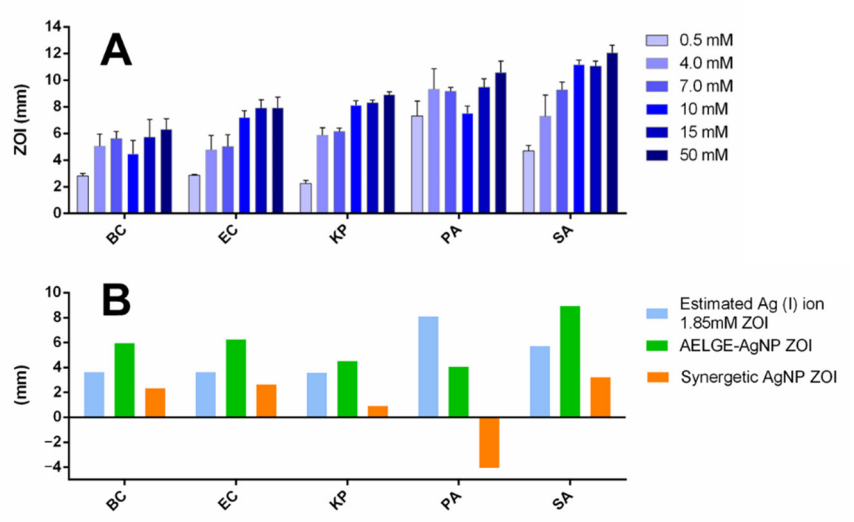

Figure 5. ZOI of AELGE-AgNPs compared to free Ag^+ ion ZOI: (**A**) A 12 µL volume of Ag^+ ion solution at various concentrations (0.50 mM, 4.0 mM, 7.0 mM, 10 mM, 15 mM, and 50 mM) was applied to 6 mm discs on petri dishes cultured with bacteria. (*Burkholderia cenocepacia* K-56 (BC), *Escherichia coli* HB101 K-12 (EC), *Klebsiella pneumoniae* ST258 (KP), *Pseudomonas aeruginosa* PAO1 (PA), *Staphylococcus aureus* USA300 (SA)) (**B**) The average ZOI of AELGE-AgNPs for each bacterium was compared to the estimated ZOI of a 1.85 mM free Ag^+ ion solution, containing the same quantity of silver in the tested AELGE-AgNP solution.

3.4. Selective Antibacterial Activity of AELGE-AgNPs

The selective antibacterial activity of AELGE-AgNPs was observed primarily in their enhanced inhibition against Methicillin-resistant SA (MRSA) (Figure 5). Among the five bacterial strains tested, AELGE-AgNPs produced the largest zone of inhibition (ZOI) against MRSA, suggesting selective antibacterial efficacy. It is also surprising that

AgNPs normally work less effectively than Ag^+ ions against Gram-positive bacteria such as MRSA due to their thick peptidoglycan layer, which acts as a barrier and limits nanoparticle penetration [20], yet AELGE-AgNPs exhibited superior activity. The potential mechanism behind this selective inhibition could be attributed to the higher binding affinity of AELGE-AgNPs to MRSA [21]. This selective binding may increase the localized concentration of nanoparticles on the bacterial surface, thereby enhancing membrane disruption and inhibiting bacterial growth [22]. The calculated ZOI area (ZOIA) further supported this observation, as AELGE-AgNPs were more effective in inhibiting MRSA than any other treated bacteria, compared to the equivalent concentration of free Ag^+ ions (Figure S6). This suggests that the unique capping agent surface properties of AELGE-AgNPs allow for stronger interaction with MRSA, potentially due to selective cell binding interactions, which induce a higher inhibitory effect on the growth of SA selectively.

A one-way analysis of variance (ANOVA) was conducted to assess the antibacterial specificity of the synthesized silver nanoparticles (AgNPs) by comparing the mean zone of inhibition (ZOI) among five bacterial strains: *Burkholderia cenocepacia* (BC), *Escherichia coli* (EC), *Klebsiella pneumoniae* (KP), *Pseudomonas aeruginosa* (PA), and *Staphylococcus aureus* (SA). The ANOVA analysis revealed a statistically significant difference in ZOI values across the bacterial groups ($F = 10.52$, $p = 0.00029$; $p < 0.001$), indicating that the efficacy of the AgNPs varied depending on the bacterial species. A post hoc Tukey HSD test was then performed to determine which specific pairs of groups differed significantly. The results demonstrated that all comparisons involving SA were statistically significant at the $p < 0.01$ level. Specifically, SA exhibited significantly larger ZOI values when compared to KP, PA, BC, and EC. This confirms that the AgNPs are significantly more effective against *Staphylococcus aureus* than against the other tested bacterial strains. The average ZOI for SA (9.16 ± 1.11 mm) was significantly greater than those observed for the other species, supporting the conclusion that these AgNPs display selective antibacterial activity. The enhanced susceptibility of SA may be due to differences in bacterial surface structures or charge properties that promote more effective interaction or penetration by the AgNPs, particularly considering the nature of the protein or peptide-based capping agents used in bioreduction synthesis. Further mechanistic studies are necessary to clarify the molecular basis for this selective efficacy. AELGE-AgNPs were also found to be more effective in inhibiting the growth of the five bacteria compared to both the Citrate-AgNPs + AELGE group and the Citrate-AgNPs group. The inhibitory effect of AELGE-AgNPs against SA was significantly more pronounced than against the other four bacterial strains, compared to the Citrate-AgNPs + AELGE group and the Citrate-AgNPs group (Figure 6).

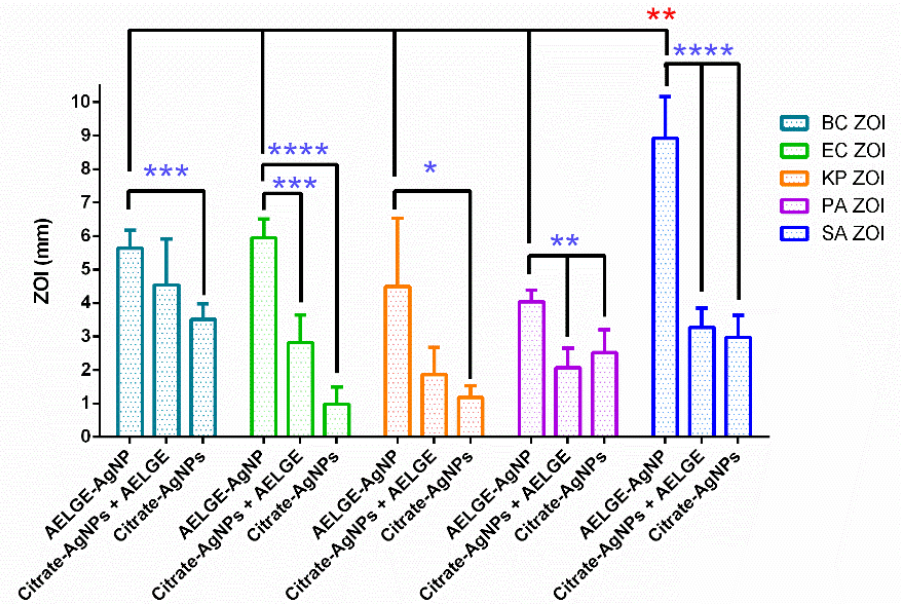

Figure 6. Comparison of Zone of Inhibition from AELGE-AgNPs Against Five Bacterial Strains: The synthesized AELGE-AgNPs exhibited the largest statistically significant zone of inhibition (ZOI) against Staphylococcus aureus (USA300) at 37 °C among the five tested strains: *Burkholderia cenocepacia* K-56, *Klebsiella pneumoniae* ST258, *Pseudomonas aeruginosa* PAO1, *Staphylococcus aureus* (USA300), and *Escherichia coli* HB101 K-12. The ZOIs produced by AELGE-AgNPs were significantly larger than those observed for both the Citrate-AgNPs + AELGE group and the Citrate-AgNPs group. Blue asterisks denote statistical significance based on unpaired *t*-tests, while red asterisks indicate significance determined by ANOVA followed by Tukey's HSD test. Results are expressed using asterisks to indicate significance levels as follows: $p > 0.05$ was considered not significant (ns); $0.01 < p \leq 0.05$ was considered significant (*); $0.001 < p \leq 0.01$ was very significant (**); $0.0001 < p \leq 0.001$ was highly significant (***); and $p \leq 0.0001$ was extremely significant (****).

3.5. Role of Reactive Oxygen Species ROS in Antibacterial Activity

One of the critical antibacterial mechanisms of silver nanoparticles (AgNPs) is their ability to generate reactive oxygen species (ROS), which play a central role in inducing oxidative stress within bacterial cells [23,24]. ROS, including superoxide anions (O_2^-), hydroxyl radicals (·OH), and hydrogen peroxide (H_2O_2), are highly reactive molecules that disrupt essential cellular components such as phospholipid membranes, intracellular proteins, and nucleic acids [25]. This oxidative damage ultimately compromises the structural and functional integrity of bacterial cells, leading to cell death [26]. The generation of ROS by AgNPs is closely linked to their physicochemical properties, particularly particle size and surface characteristics [27]. It is well established that AgNPs with diameters smaller than 10 nm are especially effective at ROS generation due to their increased surface-area-to-volume ratio, which facilitates more extensive interactions with molecular oxygen and intracellular biomolecules [28].

In our study, transmission electron microscopy (TEM) revealed that a substantial proportion of AELGE-AgNPs fall within or below this critical size range. The histogram analysis (Figure S5) supports this observation, indicating a prominent population of particles between 3 and 11 nm. Moreover, the protein/peptide-based capping agents derived from the aqueous Eastern lubber grasshopper extract (AELGE) may synergistically enhance ROS-mediated antibacterial activity. These bioorganic molecules stabilize the AgNPs and may facilitate stronger interactions with bacterial cell surfaces, thereby increasing nanoparticle retention and proximity to the bacterial envelope. This enhanced contact promotes localized ROS accumulation and potentiates oxidative damage [29]. Additionally, it might be possible that specific membrane-associated proteins on MRSA cells may possess high affinity toward glycoprotein residues or peptide motifs in the AELGE capping agents [17]. Such affinity-driven interactions may facilitate stronger adherence of AELGE-AgNPs to MRSA cell walls, increasing localized Ag^+ ion concentration and enhancing ROS-related membrane damage [30]. However, to directly quantify and confirm ROS levels generated by AELGE-AgNPs, future experiments will employ fluorescence-based assays such as DCFH-DA. Such measurements will provide quantitative validation of ROS-mediated oxidative stress and correlate it with antimicrobial efficacy.

Together, the small size of AELGE-AgNPs and their bioactive surface chemistry likely contribute to the pronounced antibacterial activity observed against Methicillin-resistant *Staphylococcus aureus* (MRSA) in our disk diffusion assays. The elevated ROS production, facilitated by both physical and biochemical properties of the nanoparticles, represents a key mechanism underlying the selective and enhanced antibacterial efficacy of AELGE-AgNPs. To sum up, our selective inhibition of MRSA by AELGE-AgNPs contrasts most AgNP studies that show broader-spectrum antibacterial activity [21,22]. This specificity may be due to the unique binding affinity of protein/peptide capping agents in our extract, consistent with Ferreira et al. 2023 [20], who showed that capping agents affect bacterial interaction significantly.

4. Conclusions

We successfully synthesized silver nanoparticles (AgNPs) using an aqueous extract of the Eastern lubber grasshopper (*Romalea microptera*) as a natural reducing and capping agent. The resulting AELGE-AgNPs exhibited strong and selective antibacterial activity against methicillin-resistant *Staphylococcus aureus* (MRSA), outperforming both citrate-AgNPs (with or without AELGE) and free Ag^+ ions. This selectivity is likely due to protein-based capping agents in the extract, which may enhance binding to MRSA cell surfaces and increase antibacterial potency. Our results suggest that insect-derived, protein-rich extracts offer a promising green method for producing targeted antimicrobial nanomaterials, with advantages such as ease of production, safety, cost-effectiveness, selective antibacterial properties, and environmentally friendly processes, ultimately reducing potential side effects. Future work will include XRD analysis, ROS quantification assays (such as DCFH-DA), dynamic light scattering (DLS), and zeta potential measurements for nanoparticle stability analysis, proteomic profiling of AELGE-bound proteins.

Supplementary Materials

The following supporting information can be found at: https://www.sciepublish.com/article/pii/626, Figure S1. A female Eastern lubber grasshopper (ELG) (scientific name: *Romalea microptera*): (A) Top-down view of the ELG: The Eastern lubber grasshopper (*Romalea microptera*) is a large grasshopper, distinguished by its vivid and striking coloration. The ELG has a distinctive coloration pattern, featuring a primarily black body with vibrant yellow, orange, and red markings on the wings. The forewings (tegmina) are short. (B) Lateral view of the ELG: The head is large with prominent compound eyes and short, robust antennae. The thorax is broad and shield-like, adorned with a colorful pattern. The abdomen is similarly colorful and stout. The legs are thick and strong, with the hind legs adapted more for

walking than jumping. Figure S2. Proteins in Aqueous Eastern lubber grasshopper (ELG) extract (AELGE): The same AELGE sample was run on an SDS polyacrylamide gel (lanes 1 and 2). The protein bands were unclear, and most of the proteins in the AELGE sample failed to penetrate the SDS polyacrylamide gel, remaining at the top of the wells. A possible explanation is that the AELGE proteins are mostly glycoproteins, which may have difficulty penetrating the SDS gel. Figure S3. UV-Vis spectra of AELGE-AgNPs and Citrate-AgNPs: The broad peak in the UV-Vis spectrum of AELGE-AgNPs, located around 440 nm within the 400–600 nm range, suggests an average particle size of approximately 40–50 nm. Similarly, the broad peak of Citrate-AgNPs, centered around 455 nm, indicates an average size of approximately 60 nm (Paramelle et al., 2014). Figure S4. Scanning Electron Microscope (SEM) images of AELGE-AgNPs and Citrate-AgNPs: (A) Fairly uniform-sized AELGE-AgNPs are observed in the SEM images. (B) AELGE-AgNPs are shown at a greater magnification in the SEM image. (C) Fairly uniform-sized citrate-AgNPs are observed in the SEM images as well. (D) Citrate-AgNPs are shown at a greater magnification in the SEM image. (B) AELGE-AgNPs are shown at a greater magnification in the SEM image. Figure S5. Histogram of particle sizes for AELGE-AgNPs and Citrate-AgNPs observed in the TEM images in Figure 3C,D: (A) AELGE-AgNPs exhibit fairly uniform and small sizes, mostly ranging from 3 to 11 nm, as shown in Figure 3C. (B) Citrate-AgNPs display a broader size distribution, ranging from 6 to 42 nm, as seen in Figure 3D. Figure S6. EDX Data of AELGE-AgNPs: The AELGE-AgNPs were synthesized and capped with biological molecules containing carbon, nitrogen, and oxygen elements. This indicates that the Eastern lubber grasshopper extract includes proteins, polypeptides, and other common nitrogen/oxygen-containing organic compounds. (Note: aluminum tape under the samples detected an aluminum signal.) Figure S7. Estimated free Ag^+ ion ZOI by mathematical calculations with average ZOI (mm) (*y* axis) and applied Ag^+ ion concentration (mM) (*x* axis). Figure S8. Estimated AELGE-AgNP ZOI area (ZOIA) Enhancement compared to free Ag^+ ions by mathematical calculations with ZOIA (mm^2) (*y* axis) and applied Ag^+ ion concentration (mM) (*x* axis).

Acknowledgments

The authors express their gratitude to the Louisiana Biomedical Research Network (LBRN) for seed funding provided through NIH Award Number 00002063438, which facilitated the initiation of this project. Partial support was also provided through the Louisiana Biomedical Research Network's pilot project, funded by the National Institute of General Medical Sciences (NIGMS) Grant 8P20GM103424 and the Louisiana Board of Regents Support Fund. Furthermore, the College of Science and Technology at Southeastern Louisiana University partially supported this research through its internal research fund. We also thank Dongmei Cao at Louisiana State University for her assistance with TEM/SEM imaging.

Author Contributions

Conceptualization, J.L.C. and L.H.S.; Methodology, J.L.C.; Validation, J.L.C., L.H.S., W.J.D., Y.Q., W.Y. and H.M.S.G.; Formal Analysis, J.L.C., L.H.S.; Investigation, J.L.C.; Resources, J.L.C. and L.H.S.; Data Curation, J.L.C. and L.H.S.; Writing Original Draft Preparation, J.L.C.; Writing Review & Editing, J.L.C., L.H.S. and W.J.D.; Visualization, J.L.C.; Supervision, J.L.C.; Project Administration, J.L.C.; Funding Acquisition, J.L.C.

Ethics Statement

Not applicable.

Informed Consent Statement

Not applicable.

Data Availability Statement

Data supporting the findings of this study are available from the corresponding author upon reasonable request.

Funding

The authors acknowledge the Louisiana Biomedical Research Network (LBRN) for providing seed funding through NIH Award Number 00002063438, which enabled the initiation of this project. Partial support was also provided through the Louisiana Biomedical Research Network's pilot project, funded by the National Institute of General Medical Sciences (NIGMS) Grant 8P20GM103424 and the Louisiana Board of Regents Support Fund.

Furthermore, this research was partially supported by the internal research fund of the College of Science and Technology at Southeastern Louisiana University.

Declaration of Competing Interest

The authors declare that they have no known competing financial interests or personal relationships that could have appeared to influence the work reported in this paper.

References

1. Chambers HF, Deleo FR. Waves of resistance: Staphylococcus aureus in the antibiotic era. Nature reviews. *Microbiology* **2009**, *7*, 629–641. doi:10.1038/nrmicro2200.
2. CDC. Staph Infections Can Kill. Centers for Disease Control and Prevention. Available online: https://www.cdc.gov/vitalsigns/staph/index.html (accessed on 24 July 2024).
3. Antimicrobial resistance. Available online: https://www.who.int/antimicrobial-resistance/en/ (accessed on 27 September 2024).
4. Lara HH, Ayala-Núñez NV, Ixtepan Turrent LDC, Rodríguez Padilla C. Bactericidal effect of silver nanoparticles against multidrug-resistant bacteria. *World J. Microbiol. Biotechnol.* **2010**, *26*, 615–621. doi:10.1007/s11274-009-0211-3.
5. Xiu Z-M, Zhang Q-B, Puppala HL, Colvin VL, Alvarez PJJ. Negligible particle-specific antibacterial activity of silver nanoparticles. *Nano Lett.* **2012**, *12*, 4271–4275. doi:10.1021/nl301934w.
6. Ansari MA, Asiri SMM, Alzohairy MA, Alomary MN, Almatroudi A, Khan FA. Biofabricated fatty acids-capped silver nanoparticles as potential antibacterial, antifungal, antibiofilm and anticancer agents. *Pharmaceuticals* **2021**, *14*, 139. doi:10.3390/ph14020139.
7. Kalimuthu K, Suresh Babu R, Venkataraman D, Bilal M, Gurunathan S. Biosynthesis of silver nanocrystals by Bacillus licheniformis. *Colloids Surfaces. B Biointerfaces* **2008**, *65*, 150–153. doi:10.1016/j.colsurfb.2008.02.018.
8. Cho JL, Liu S, Wang P. Green chemical synthesis of size-controlled gold nanodisk governed by hydrophilic protein/peptide-rich aqueous extract from American cockroach, Periplaneta americana. *BioNanoScience* **2023**, *13*, 167–175. doi:10.1007/s12668-022-01049-y.
9. Cho JL, Liu S, Wang P, Park J-W, Choi D, Evans RE. Silver nanoparticles induced with aqueous black carpenter ant extract selectively inhibit the growth of Pseudomonas aeruginosa. *Biotechnol. Lett.* **2023**, *45*, 811–821. doi:10.1007/s10529-023-03386-8.
10. Eastern Lubber Grasshopper—Romalea Guttata (Houttuyn). Available online: https://entnemdept.ufl.edu/creatures/orn/lubber.htm (accessed on 28 September 2024).
11. Ramos-Elorduy J, Moreno JMP, Prado EE, Perez MA, Otero JL, de Guevara OL. Nutritional value of edible insects from the state of Oaxaca, Mexico. *J. Food Compos. Anal. Off. Publ. United NationsUniv. Int. Netw. Food Data Syst.* **1997**, *10*, 142–157. doi:10.1006/jfca.1997.0530.
12. Bukkens SGF. The nutritional value of edible insects. *Ecol. Food Nutr.* **1997**, *36*, 287–319. doi:10.1080/03670244.1997.9991521.
13. Paramelle D, Sadovoy A, Gorelik S, Free P, Hobley J, Fernig DG. A rapid method to estimate the concentration of citrate capped silver nanoparticles from UV-visible light spectra. *Analyst* **2014**, *139*, 4855–4861. doi:10.1039/c4an00978a.
14. Nandiyanto ABD, Ragadhita R, Fiandini M. Interpretation of Fourier transform infrared spectra (FTIR): A practical approach in the polymer/plastic thermal decomposition. *Indones. J. Sci. Technol.* **2022**, *8*, 113–126. doi:10.17509/ijost.v8i1.53297.
15. Kalimuthu K. Biosynthesis of silver nanoparticles using the fungus Fusarium oxysporum and its potential antibacterial activity. *J. Biol. Chem.* **2008**, *11*, 114–124.
16. Gharibshahi L, Saion E, Gharibshahi E, Shaari AH, Matori KA. Structural and optical properties of Ag nanoparticles synthesized by thermal treatment method. *Materials* **2017**, *10*, 402. doi:10.3390/ma10040402.
17. Carvalho GC, Sábio RM, de Cássia Ribeiro T, Monteiro AS, Pereira DV, Ribeiro SJL, et al. Highlights in mesoporous silica nanoparticles as a multifunctional controlled drug delivery nanoplatform for infectious diseases treatment. *Pharm. Res.* **2020**, *37*, 191. doi:10.1007/s11095-020-02917-6.
18. Mourdikoudis S, Pallares RM, Thanh NTK. Characterization techniques for nanoparticles: comparison and complementarity upon studying nanoparticle properties. *Nanoscale* **2018**, *10*, 12871–12934. doi:10.1039/c8nr02278j.
19. Sharma NK, Vishwakarma J, Rai S, Alomar TS, AlMasoud N, Bhattarai A. Green route synthesis and characterization techniques of silver nanoparticles and their biological adeptness. *ACS Omega* **2022**, *7*, 27004–27020. doi:10.1021/acsomega.2c01400.
20. Ferreira AM, Vikulina A, Loughlin M, Volodkin D. How similar is the antibacterial activity of silver nanoparticles coated with different capping agents? *RSC Adv.* **2023**, *13*, 10542–10555. doi:10.1039/d3ra00917c.
21. Gurunathan S, Han JW, Kwon D-N, Kim J-H. Enhanced antibacterial and anti-biofilm activities of silver nanoparticles against Gram-negative and Gram-positive bacteria. *Nanoscale Res. Lett.* **2014**, *9*, 373. doi:10.1186/1556-276x-9-373.

22. Bondarenko O, Ivask A, Käkinen A, Kurvet I, Kahru A. Particle-cell contact enhances antibacterial activity of silver nanoparticles. *PloS ONE* **2013**, *8*, e64060. doi:10.1371/journal.pone.0064060.
23. Rai M, Yadav A, Gade A. Silver nanoparticles as a new generation of antimicrobials. *Biotechnol. Adv.* **2009**, *27*, 76–83. doi:10.1016/j.biotechadv.2008.09.002.
24. Ebrahiminezhad A, Barzegar Y, Ghasemi Y, Berenjian A. Green synthesis and characterization of silver nanoparticles using Alcea rosea flower extract as a new generation of antimicrobials. *Chem. Ind. Chem. Eng. Q.* **2017**, *23*, 31–37. doi:10.2298/ciceq150824002e.
25. Marambio-Jones C, Hoek EMV. A review of the antibacterial effects of silver nanomaterials and potential implications for human health and the environment. *J. Nanopartic. Res. Interdiscip. Forum Nanoscale Sci. Technol.* **2010**, *12*, 1531–1551. doi:10.1007/s11051-010-9900-y.
26. Durán N, Marcato PD, Alves OL, Souza GIHD, Esposito E. Mechanistic aspects of biosynthesis of silver nanoparticles by several Fusarium oxysporum strains. *J. Nanobiotechnol.* **2005**, *3*, 8. doi:10.1186/1477-3155-3-8.
27. Li W-R, Xie X-B, Shi Q-S, Zeng H-Y, Ou-Yang Y-S, Chen Y-B. Antibacterial activity and mechanism of silver nanoparticles on *Escherichia coli*. *Appl. Microbiol. Biotechnol.* **2010**, *85*, 1115–1122. doi:10.1007/s00253-009-2159-5.
28. Pal S, Tak YK, Song JM. Does the antibacterial activity of silver nanoparticles depend on the shape of the nanoparticle? A study of the Gram-negative bacterium *Escherichia coli*. *Appl. Environ. Microbiol.* **2007**, *73*, 1712–1720. doi:10.1128/AEM.02218-06.
29. Zhang X-F, Liu Z-G, Shen W, Gurunathan S. Silver nanoparticles: Synthesis, characterization, properties, applications, and therapeutic approaches. *Int. J. Mol. Sci.* **2016**, *17*, 1534. doi:10.3390/ijms17091534.
30. Dakal TC, Kumar A, Majumdar RS, Yadav V. Mechanistic basis of antimicrobial actions of silver nanoparticles. *Front. Microbiol.* **2016**, *7*, 1831. doi:10.3389/fmicb.2016.01831.